Experimental Investigation of Droplet Dynamics and Spray Atomization inside Thermostatic Expansion Valves

M. Huo and C. F. Lee*
Department of Mechanical Science and Engineering
University of Illinois at Urbana-Champaign
1206 West Green Street
Urbana, Illinois 61801, USA

Abstract

Experimental investigation on spray atomization and droplet dynamics inside a thermostatic expansion valve (TEV) was conducted. A needle and an orifice were copied from a commercial TEV and machined to be mounted inside a chamber with optical access so that the flow inside the TEV is simulated and visualized at the same time. The break-up and atomization of the refrigerant were documented near the downstream of the orifice under different feed conditions on micro-second scale. A Phase Doppler Anemometry (PDA) system was used later to measure the size of atomized refrigerant droplets. It is found that spray impingement is inevitable and crucial to the atomization. Under steady-state operation, liquid film was seen formed on the needle plate and caused droplets splashed from plate, which will further have an effect on the droplets size. The before impact and after impact droplets were characterized by PDA system and for studying the impingement. In addition, the impact of the needle geometry inside the valve on refrigerant atomization has also been investigated.

* Corresponding author: Chia-fon F. Lee <cflee@illinois.edu>

Introduction

The thermostatic Expansion valve (TEV) or electronic expansion valve (EEV) are commonly used in air conditioning or refrigeration systems as flow regulating devices. Refrigerant passing through the valve is throttled and therefore the high pressure side is separated from the low pressure side in a system. The decisive advantage of TEV and EEV over the traditional expansion devices such as capillary tubes is their capability of adjusting the mass flow rate according to the superheat degree inside the evaporator. Such advantage, however, also induced problems such as "valve hunting", or poor two phase refrigerant distribution inside evaporator circuits [1-2]. Many investigators have tried to model the mass flow rate based on the experimental data related to valve inlet and outlet and various correlations have been proposed [3-6]. Unfortunately, they were unable to visualize the actual throttling process inside the valve, and consequently the refrigerant atomization and its impact are rarely found in the open literature.

The objective of this study is to build an "optical valve" so that the refrigerant spray can be visualized and measured using laser diagnostics. The details of the experiment setup will be given in the later section. It should be pointed out that the spray and atomization process inside the TEV/EEV is complicated and involves many physical processes such as droplet breakup, flash boiling, spray wall impact, etc. From the backlit photography results, spray wall impact is found to be crucial to the refrigerant atomization under the current nozzle configuration, since most of the liquid refrigerant is unable to be fully atomized before impinging on the needle plate. Homogeneous two phase flow featured by fully atomized small droplets is desirable in the system operation while large drops and liquid films inside the valve resulted from poor atomization can cause problems such as valve hunting and poor refrigerant distribution in the evaporator as aforementioned. Therefore, the behavior of the drops induced by the spray wall impact is of great importance to the TEV/EEV performance.

Spray plate nozzle has been studied by a number of investigators in the past decades [7-9]. Most of these studies used water or fuel as the working fluid, while refrigerant has been rarely studied. In general, there are two outcomes of droplet impinging on the solid surface, the droplet will either deposit on the surface and form a liquid film or splash and break into secondary droplets. A number of researchers had attempted to establish correlations for the deposition-splashing limit using Weber number ($We=\rho_L U^2/\sigma$, U is jet velocity). These experiments, however, were restricted to normal impact of a single droplet onto dry or wetted surface where the impingement conditions can be carefully controlled [10-13]. Tropea et al [14,15] performed experiments on drop impingement in a spray and they found the resulted drop behavior differed significantly from that of an isolated single droplet. They proposed new models where correlations are based on the mean statistics of the spray rather than on a single droplet. Other models can be found in terms of the drops size and velocity correlation [7-9]. The experiment results of Mccreery et al [7] showed a mean drop diameter dependency on pressure to approximately -0.3 power for a spray plate nozzle, which was a reasonable agreement with Fraser's correlation [8], in which the drop size produced by a low viscosity liquid sheet can be expressed as

$$d \propto (\rho_L/\rho_G)^{1/6}\sigma^{1/3}P^{-1/3} \qquad 1)$$

where P is the gauge pressure.

In summary, the spray wall impact will greatly affect the refrigerant atomization inside a TEV/EEV. Although studied in many other applications, the spray wall impact of refrigerant is rarely investigated. Also, pressure is found to be an important parameter regarding the drop size distribution. In this article, the refrigerant atomization in an orifice needle plate is visualized and measured. Results include the short duration (3μs) photographs of refrigerant spray wall impingement, and drops size distribution measured by PDA system. The impact of the pressure is discussed and correlations are presented.

Experiment Setup

To simulate the real working conditions of TEV and EEV, a refrigerant loop is introduced as shown in Fig. 1. R134a, a commonly used refrigerant in air conditioning systems which has a formula CH2FCF3, is chosen as the working fluid in this study. The gear pump is used to provide the pressure head to R134a; a recycle bypass is then introduced to control the pressure of the fluid. A resistance heater coupled with a variac is used to heat the refrigerant. The temperature and pressure of the upstream refrigerant (before entering the test section) can then be precisely controlled and measured. The measuring devices are listed in Table1. After the test section, two-phase R134a is condensed in a plate heat exchanger by cooling water. A specific R134a receiver is mounted before the pump to avoid cavitations inside the gear pump before the cycle starts again.

The test section, so called as the "optical valve", is a chamber with optical access which is centered around by the laser based measuring devices. The dimension of the inlet path, orifice and needle plate of a commercial TEV were copied out and machined into an adapter which can be further mounted inside the optical chamber. A push rod, coupled with a meter head at one end penetrates through the bottom plate and can be moved vertically as illustrated in Fig. 2. The needle plate is mounted on the top of the push rod which can be aligned with the orifice using the slide jack. The configuration of the

needle/orifice nozzle is shown in Fig. 3 and the dimensions of two different nozzles are listed in Table2. The equivalence diameter D_e is defined as $D_e=d_o-d_i$. With d_o fixed and d_i changeable, the open/close of the valve can easily controlled by lifting up and down the push rod.

Backlight illumination technique was employed to investigate the spray formation and breakup processes, allowing qualitative study on the spray shapes and structure. The laser shines onto a diffuser to provide a homogenous background while the camera is placed at the other side of the chamber as shown in Fig. 4. A Phantom Research v7.0 high-speed camera was used with a frame rate of 10,000 fps and an exposure time of 3 μs; an Oxford copper vapor laser was used as the light source with a pulse rate of 10,000Hz to achieve the laser/camera synchronization.

The optical chamber has four side windows whose positions are specifically arranged to meet the requirement of the PDA system. A Dantec Dynamics PDA system was used in this study to provide a quantitative analysis of the spray inside the TEV. Dantec P60 Flow & Particle processor was used for signal processing, while an Argon Ion Laser (Stabilite 2017) by Spectra-Physics was used as the light source. Spatial adjustments were done with a Dantec manual transverse system. In this setup, the spatial profiles of droplet size were measured by a one-dimensional PDA. The beam separation was 50 mm and the laser power was 900 mW at a wavelength of 514 nm per beam. The scattering light collection lens on the Dantec receiver optical system has a focal length of 310 mm. The receiver was positioned at a scattering angle of 70° to ensure only the first order refractions were collected.

Results and Discussion

Two nozzles of different geometry have been chosen for this study. Nozzle 1 is copied from Sporlan FV series while nozzle 2 is copied from Sporlan GV series. Both TEVs are designed for small refrigeration systems such as refrigerated cases, coolers and freezers, while the former one is more desirable for external adjustment. Nozzle 1 has been mainly studied through this study while the experimental data for Nozzle 2 is still limited to this point. Therefore the results are mainly based on nozzle 1 unless specifically pointed out. The equivalence diameter of the nozzle are both fixed at 0.6 mm. Regarding the test conditions, we maintained the back pressure inside the chamber at 60 psi while increased the feeding pressure from 110 psi to 140 psi, and thus produced a pressure drop from 50 psi to 80 psi correspondingly. All the cases are characterized by the pressure drop through the orifice since this parameter is of more interest in air conditioning system.

Backlit photography

The photographs of the refrigerant spray at steady state are shown in Fig. 5. For each case, we focused on just one side of the spray and the white lines mark the orifice and needle plate in each figure. For all the cases, it can be observed that the liquid refrigerant is unable to be fully atomized before hitting on the needle plate, the resultant liquid film flows radially outward and breaks into drops after detaching from the surface. With lower pressure drop, the liquid tend to deposit on the needle plate, while more drops are splashed with higher feeding pressure and particle cluster can be clearly visualized. The increase of the feeding pressure also leads to expanded spray angle, which further resulted in a more oblique impact of the spray on the plate.

Mesh Grids for PDA measurement

The mesh grids for the PDA measurement are shown in Fig. 6. The first point closest to the orifice will be 3mm from the center of the needle. The measuring point will move from 3mm to 18mm along the radial direction with an increment of 3mm. Considering the equivalence diameter D_e of the orifice is 0.6mm, the radial distance of the measuring point from the center will be $5D_e$, $10D_e$, $15D_e$, $20D_e$,$25D_e$ and $30D_e$ correspondingly. In the axial direction, the measuring points are all 1mm from the poppet base for both nozzles, which will be about $4.5D_e$ from the orifice. It should be pointed out that unlike the studies on the fuel injection systems where the measuring points can be taken at spray fully developed region (e.g. 100D downstream), limited expansion room (usually in the order of ~1cm^3) causing impingement from the poppet base features the spray inside a TEV or EEV. Therefore, the points chosen for PDA measurement are inevitable close to the orifice in relative speaking to represent the real spray inside the expansion valve.

The problem raised from choosing points too close to the orifice is the spherical validation rate of the PDA measurement, since the PDA will reject the non-spherically particles automatically. The spherically validation are monitored and recorded all through the experiment. Preliminary results showed that even at the point closest to the orifice, the validation rate is about 80%, indicating an acceptable reliability on the data. The spherically validation rate increase to 90% or above for the rest measuring points, indicating the spray drops become finer and more spherical shaped. Meanwhile, since the spray is at steady state, the sampling rate requirement will not be as high as those done in injection experiments (e.g. usually 1000Hz or above) since the injection duration is extremely short and only with a high sampling rate can people collect enough particle samples for analysis. For this study, the sample rate is kept in an order of ~100Hz; no measurements were taken when the sampling rate is below 50Hz, though. A total amount of 5000 particle samples are collected for each case so that analysis can be made on a statistical base.

Radial distribution

The radial distributions of the drops size with different pressure drop are shown in Fig. 7 All the measured samples' diameter are sorted into a bin of 2μm and plotted against its normalized frequency count, or count percentage. Each curve represents the measurement at a single point. It is observed that under certain feeding pressure, the distribution variation for different points along the radial direction is not apparent, most points share similar peak value, indicating similar drop diameter ranges. The most remarkable observation is that at the furthest point where r/D_e = 30 for Δp = 50 psi and 60 psi, the curves do not go all the way down to zero, indicating particles with large drop diameter are detected. The possible explanation is that the drop coalescence takes place at the radial downstream since liquid ligaments were visualized splashed from the edge of the needle plate as shown in Fig. 5. With the presence of the liquid ligaments and particle cluster, it is highly possible that the drops coalesced and merged to form larger drops at downstream.

To further evaluate the drops size distribution along the radial direction, the drops mean diameter D10 and Sauter mean diameter D32, expressed as following, are plotted against the radial position for each feeding pressure case as shown in Fig. 8.

D10, the mean diameter: $D_{10} = \frac{1}{N}\sum_{i=1}^{N_i} n_i D_i$

D32, the SMD $D_{32} = \frac{\frac{1}{N}\sum_{i=1}^{N_i} n_i D_i^3}{\frac{1}{N}\sum_{i=1}^{N_i} n_i D_i^2}$

It is found that the drops diameter decreases with the increase of the radial distance at near downstream while increases at further downstream, which is consistent with the result in Fig. 7. For the curve fits, *r/D* signifies the radial distance from the nozzle and R is the residual. The data shows a mean diameter dependency and Sauter mean diameter dependency on radial distance to approximately the -0.35 power and -0.25 power respectively at the near downstream. At further downstream, the drop diameter start to increase explained by coalescence and the correlation is no longer valid.

Pressure Drop

In Fig. 7, the drops size distributions with the increase of the pressure drop through the TEV are more noticeable. It is observed that the peak value for the curves shift towards left indicating a decrease in the drops diameter. Fig. 9 illustrates the correlations between drops diameter and the feeding pressure. Again, ΔP signifies the pressure drop and R is residual in the plot.

The dependency of drop diameter on pressure drop for our data is to approximately -0.8 powers, which is considerably larger than the previous studies on spray cone nozzles (to approximately -0.3 powers). This is due to the pressure influence on both the primary drop breakup and the secondary drop breakup resulted from the impingement while the latter one is the only concern in the reviewed studies. On one hand, higher feeding pressure induces more intensive aerodynamic drag on the particles and causes more violent primary drops breakup, on the other hand, the increase of the feeding pressure also expands the spray angle resulting in more drops splashed and more violent secondary drop breakup. Such a combination effect on drops size makes the influence of feeding pressure much stronger in a needle orifice nozzle in TEV/EEV compared with other spray plate nozzles.

To further evaluate the influence of the spray impact, all the drops measured at each point are sorted into two categories by the normal velocity component of each particle measured by the PDA system: a positive velocity indicating before impact particles while a negative velocity indicating after impact. Fig. 10 and Fig. 11 shows the drops mean diameter for two different category particles and their number ratio at each point respectively. It is observed that the increase of the feeding pressure results in decrease in drop diameter for particles in both categories and this trend is more apparent at near downstream for drops before impingement. In Fig. 11, the ratio λ, which is defined as the number ratio of the impact (λ=Num aft imp/Num before impact), is a parameter of more interest in the determination of the total drop size at each point. At *r/D*=5, most of the drops coming out of the orifice haven't reached the base and resulted in a relatively smaller λ. The particles before impact, featured by large mean diameter outnumber at this point indicating that the aerodynamic breakup (primary breakup) dominates. With increase of the radial distance, λ increases sharply for all cases suggest the particles after impact outnumbers. The correlation between the pressure drop and λ is not conclusive, though highest feeding pressure results in a highest peak value.

Nozzle Geometry

Comparing the geometry of the two nozzles, it can be noticed that the valve length of nozzle 2 is smaller than nozzle 1, indicating a narrower region for the refrigerant atomization before it impinges on the wall, which resulted in a more intensive spray impingement and more liquid accumulated on the base. Consequently, the measured droplet SMD along the radial direction of nozzle 2 is noticeably larger than that of nozzle 1 as can be observed in Fig12.

Conclusion

The spray/wall impingement of R134a sprays in a needle orifice nozzle was visualized under different

feeding pressures, and the corresponding drop size distributions were measured using PDA system. The results showed that the increase of the feeding pressure induces more drops splashed from the needle plate and more violent secondary breakup, which was verified by the drops with smaller SMD in the PDA measurement.

The dependency of drop diameter on the pressure is found to be larger than previous studies on spray plate nozzle. The drops size distributions for both before impact drops and after impact drops indicate that the pressure will affect the drop size in both categories. Such a combination effect on drops size makes the influence of feeding pressure stronger in a needle orifice nozzle in TEV/EEV compared with other spray plate nozzles.

Acknowledgements

This work was sponsored by the Air Conditioning and Refrigeration Center in University of Illinois at Urbana-Champaign. The PDA system used in this work was supported by the National Science Foundation under CTS 01-16719.

References

[1] Z. R. Huellle, Heat load influence upon evaporator parameters. XIIth *Int. Refrig. Congr* (1998) Madrid. Report no.3.32.

[2] Z. Tamainot-Telto, A. Outtgarts, P. Haberschill, M. Lallemand, Behavior of a thermostatic expansion valve in non-steady state for a refrigerating machine, *Int.J.Refrig* (1996), 19(2), pp. 124-131.

[3] Y. C. Kim, D.L. O'Neal, A semi-empirical model of two-phase flow of refrigerant-R134a through short tube orifices. *Exp Therm Fluid Sci* (1994), 9(4) pp. 426-36.

[4] J. T. Choi, C.Y. Kim, A generalized correlation for two-phase flow of alternative refrigerants through short tube orifices. *Int.J.Refrig*. (2004), 27(4), pp. 393-400.

[5] S. Ma, C. Zhang, J. Chen, Z. Chen, Experimental research on refrigerant mass flow coefficient of electronic expansion valve. *Appl Therm Eng* (2005), 25, pp. 2351-2366.

[6] C. Park, H. Cho, Y. Lee, Y. Kim Mass flow characteristics and empirical modeling of R22 and R410A flowing through electronic expansion valves. *Int.J.Refrig* (2007), 30, pp.1401-1407.

[7] G. E. Mccreery, C. M. Stoots Drop formation mechanisms and size distribution for spray plate nozzles *Int J Multiphase Flow* (1996) 22,3, pp. 431-452

[8] R. P. Fraser, P. Eisenklam, N. Dombroski, D. Hasson Drop formation from rapidly moving sheets. *J AIChE* (1964)8, pp. 672-680.

[9] M. Georges, J. M. Buchlin Detailed single spray experimental measurements and one-dimensional modeling. *Int J Multiphase Flow* (1994) 20, pp.979-992.

[10] C.Bai, A.D.Gosman, Development of methodology for spray impingement simulation. *Society Automot. Eng* (1995). 950283, pp. 69–87.

[11] D. W. Stanton, C.J. Rutland. Multi-dimensional modeling of thin liquid films and spray wall interactions resulting from impinging sprays. *Int J Heat and Mass Transfer* (1998), 41, pp. 3037-3054.

[12] C. Mundo, M. Sommerfeld and C. Tropea, On the modeling of liquid sprays impinging on surfaces, *Atom Sprays* (1998), 8, 625–652.

[13] G. E. Cossali, A. Coghe and M. Marengo, The impact of a single drop on a wetted surface, *Exp. Fluids* (1997), 22, pp.463–472.

[14] S. Sivakumar and C. Tropea, Splashing impact of a spray onto a liquid film, *Phys. Fluids Lett.* (2002), 14, pp. 85–88.

[15] I. V. Roisman and C. Tropea, Fluctuating flow and jetting in a liquid layer created by an impacting spray, *Int. J. Multiphase Flow* (2005), 31, pp.179–200.

	Model	Accuracy
Thermocouple	Omega	± 0.15 C^0
Pressure	Setra 280E	± 0.11% FS
Transducer	Setra 205-2	± 0.11% FS
Flow meter	Micro Motion DH012S100SU	±2% of reading

Table 1. Measuring devices

	Nozzle 1	Nozzle 2
Orifice diameter *do* (mm)	4.57	4.57
Nozzle angle α	85	90
Nozzle length *L* (mm)	5.13	3.50
Poppet diameter *Dp* (mm)	14.32	18.12

Table 2. Nozzle dimensions

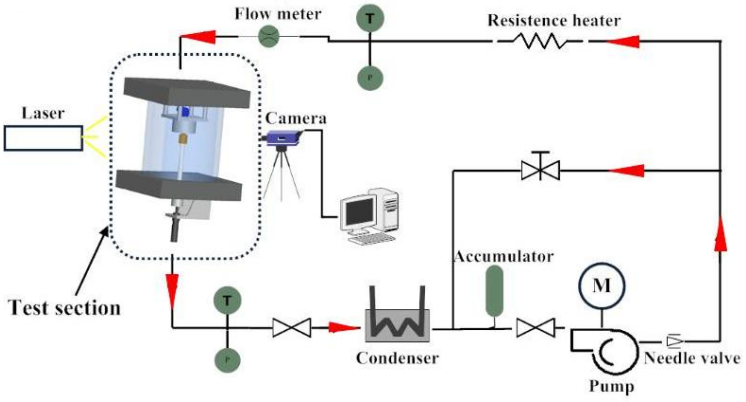

Figure 1. Refrigeration Loop

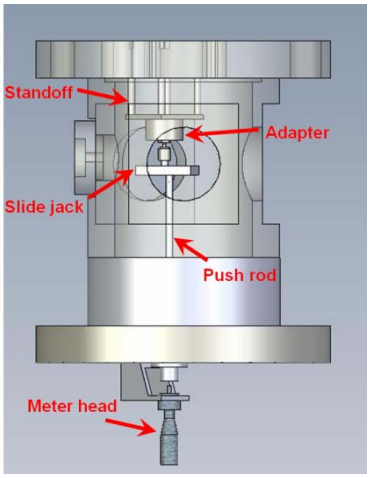

Figure 2. Optical chamber Setup

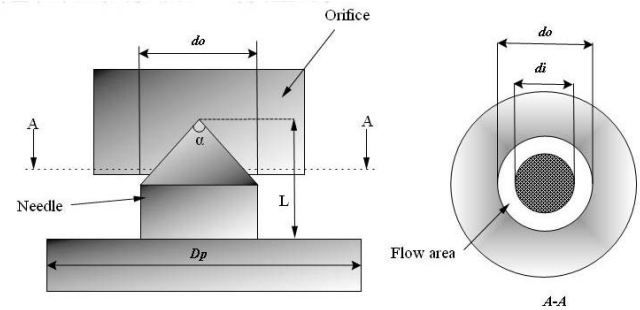

Figure 3. Nozzle configuration

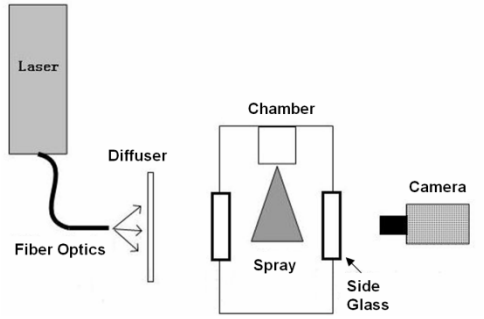

Figure 4. Backlit illumination setup

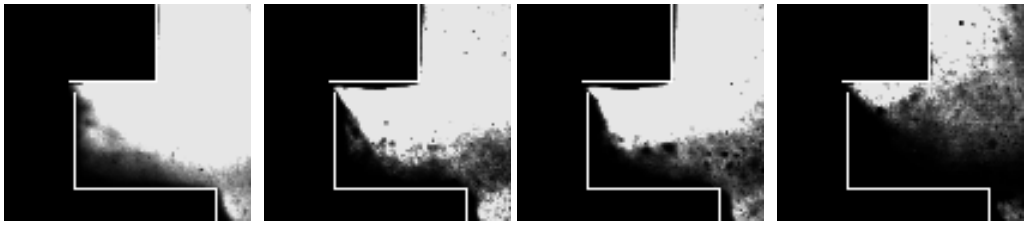

a) b) c) d)

Figure 5. Short duration photographs for refrigerant spray wall impact with differential pressure of a) 50 psi, b) 60 psi, c) 70 psi, d) 80 psi

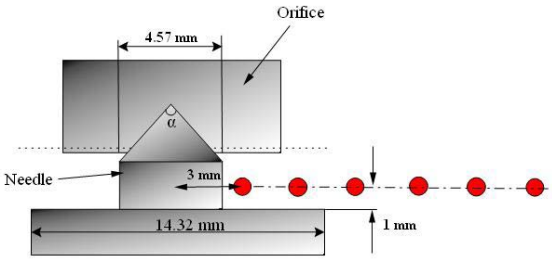

Figure 6. Mesh points for the PDA measurement

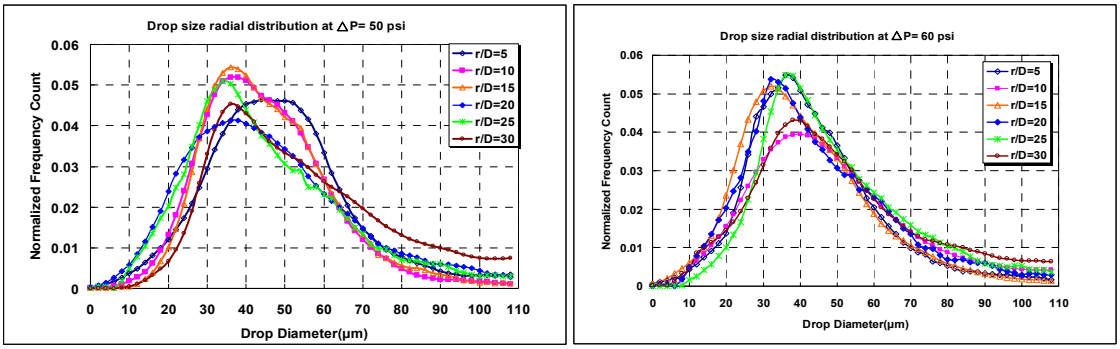

a) b)

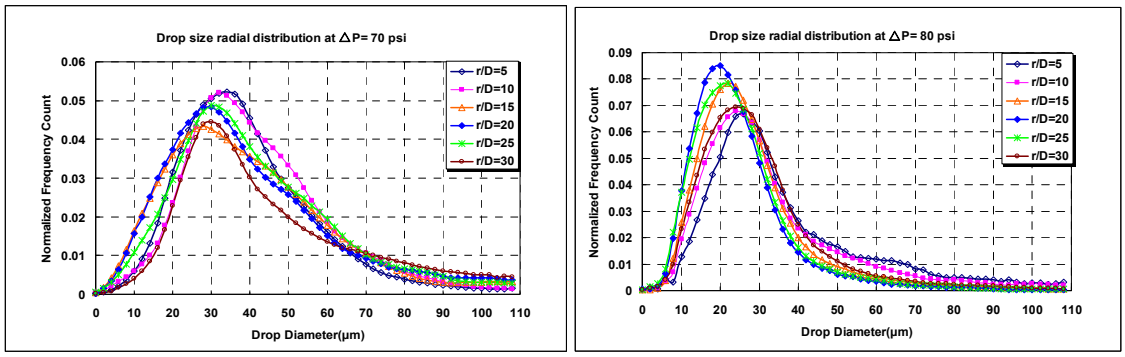

c) d)

Figure 7. Drop size radial distribution with different pressure drop through TEV a) 50 psi, b) 60 psi, c) 70 psi, d) 80 psi

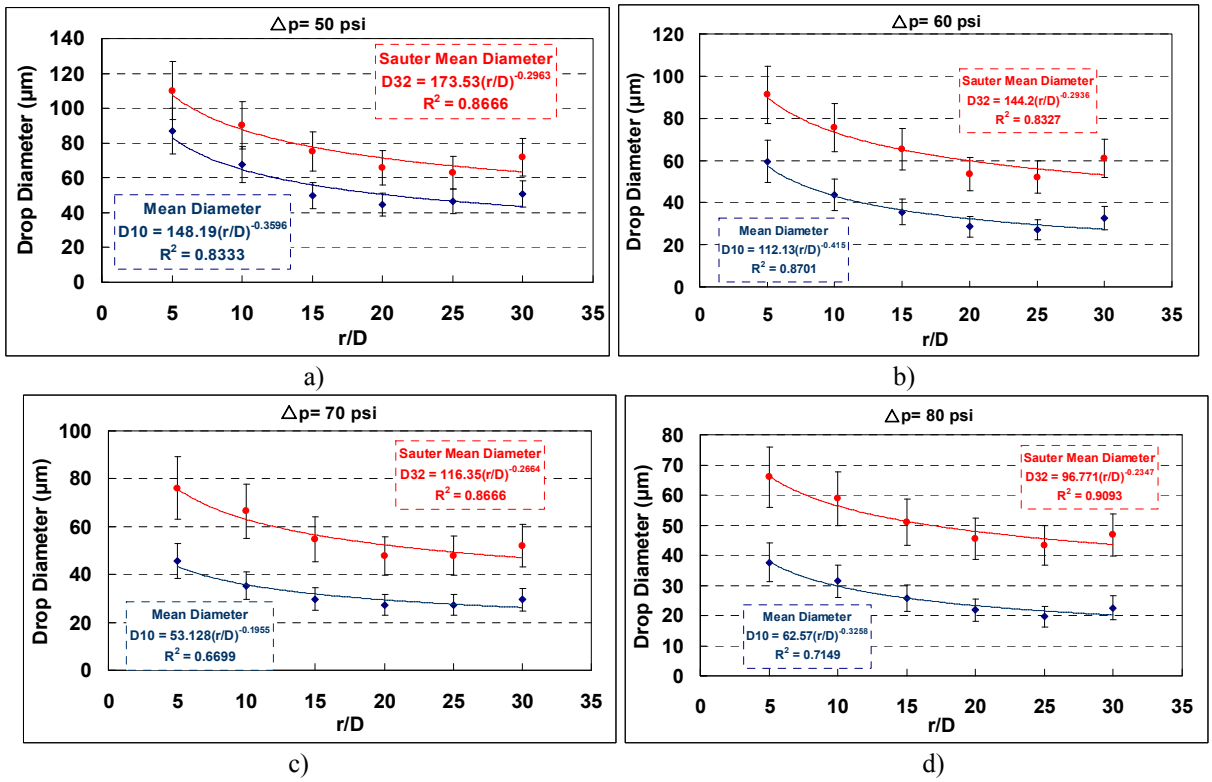

a) b)

c) d)

Figure 8. Measured Drop diameter along the radial direction with different pressure drop through TEV a) 50 psi, b) 60 psi, c) 70 psi, d) 80 psi

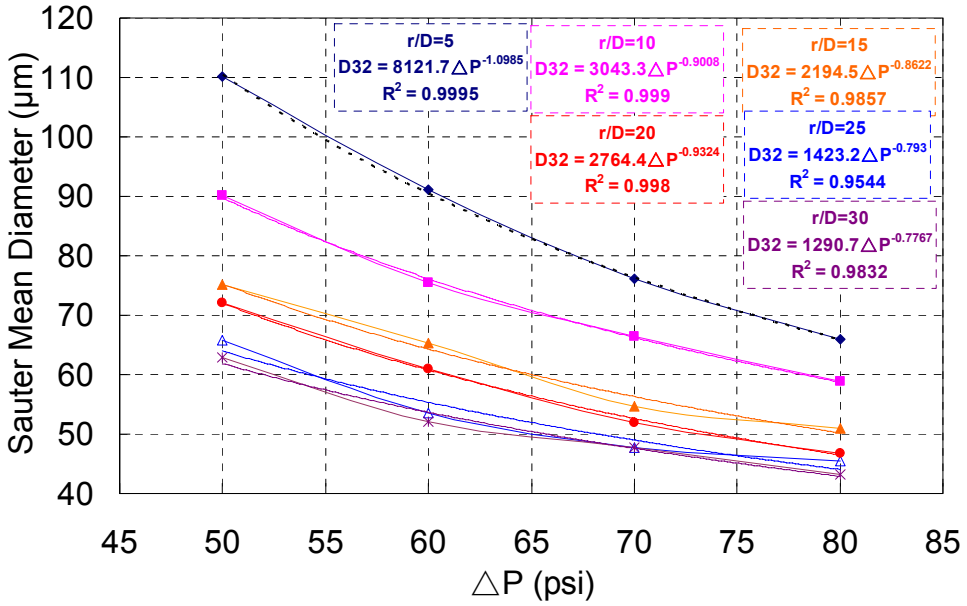

Figure 9. SMD with different pressure drop through TEV

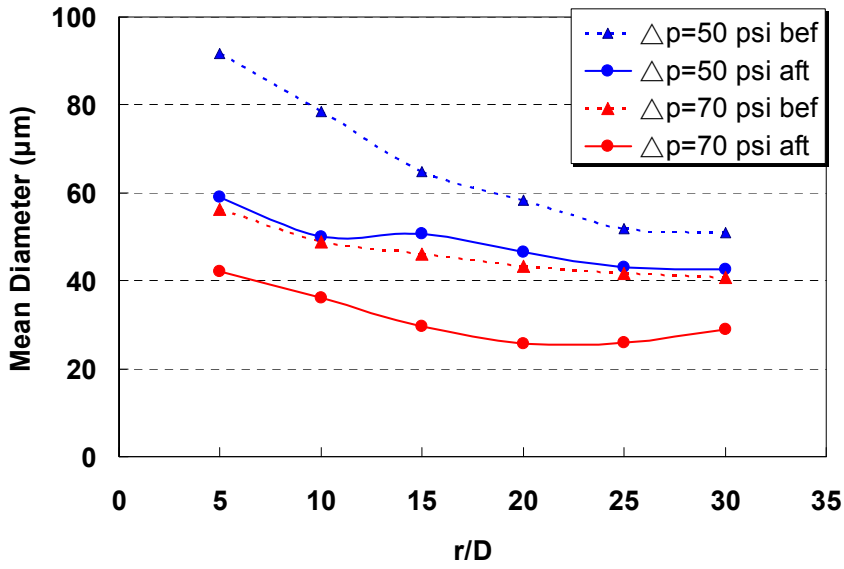

Figure 10. Droplet mean diameter before contact and after contact along the radial direction with different pressure drop through TEV

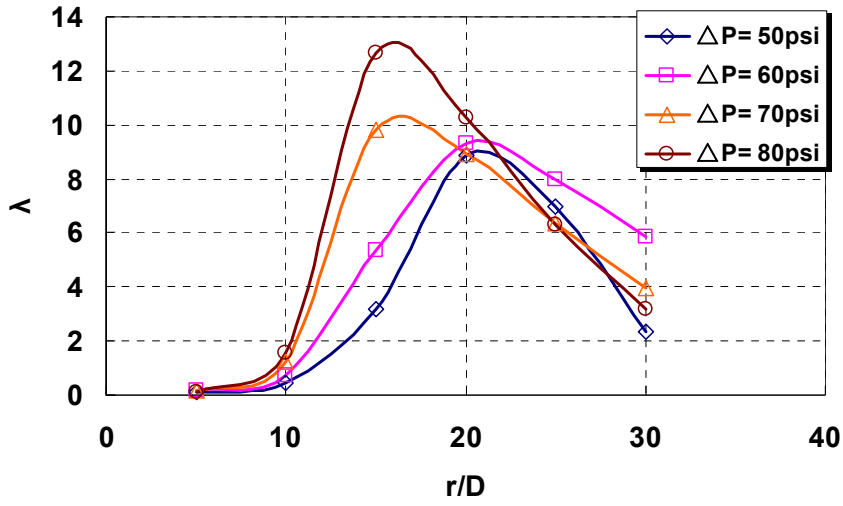

Figure 11. Number ratio along the radial direction with various differential pressures

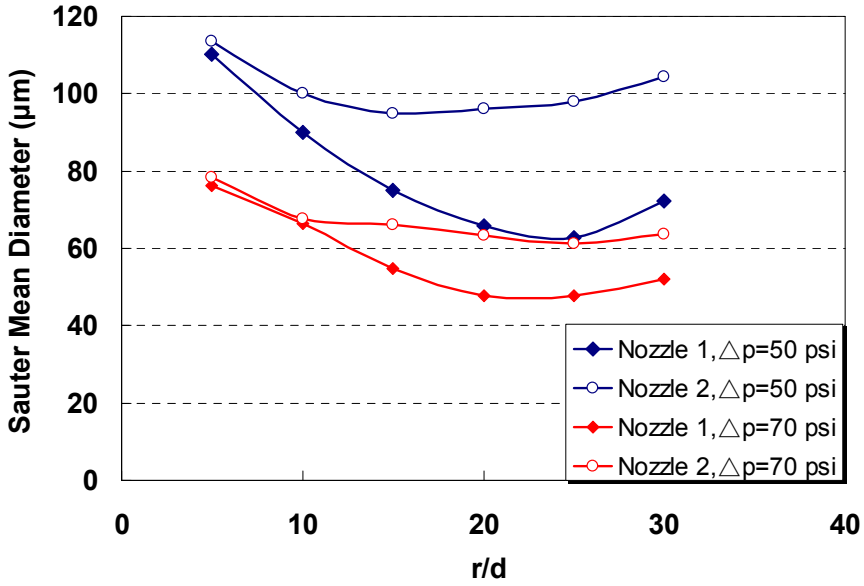

Figure 12. SMD along the radial direction of two different nozzles.